

A Lightweight Model-Driven 4D Radar Framework for Pervasive Human Detection in Harsh Conditions

Zhenan Liu

Mechanical & Mechatronics Engineering
University of Waterloo
Waterloo, Canada
z634liu@uwaterloo.ca

Amir Khajepour

Mechanical & Mechatronics Engineering
University of Waterloo
Waterloo, Canada
a.khajepour@uwaterloo.ca

George Shaker

Electrical & Computer Engineering
University of Waterloo
Waterloo, Canada
gshaker@uwaterloo.ca

Abstract—Pervasive sensing in industrial and underground environments is severely constrained by airborne dust, smoke, confined geometry, and metallic structures, which rapidly degrade optical and LiDAR-based perception. Elevation-resolved 4D millimeter-wave (mmWave) radar offers strong resilience to such conditions, yet there remains a limited understanding of how to process its sparse and anisotropic point clouds for reliable human detection in enclosed, visibility-degraded spaces. This paper presents a fully model-driven 4D radar perception framework designed for real-time execution on embedded edge hardware. The system uses radar as its sole perception modality and integrates domain-aware multi-threshold filtering, ego-motion-compensated temporal accumulation, KD-tree Euclidean clustering with Doppler-aware refinement, and a rule-based 3D classifier. The framework is evaluated in a dust-filled enclosed trailer and in real underground mining tunnels, and in the tested scenarios the radar-based detector maintains stable pedestrian identification as camera and LiDAR modalities fail under severe visibility degradation. These results suggest that the proposed model-driven approach provides robust, interpretable, and computationally efficient perception for safety-critical applications in harsh industrial and subterranean environments.

Index Terms—4D mmWave radar, human detection, harsh environments, industrial sensing, model-driven perception, pervasive safety systems, radar point clouds, underground mining.

I. INTRODUCTION

Pervasive sensing in industrial, construction, and underground environments is fundamentally constrained by visibility. Airborne dust, smoke, confined geometry, and metallic infrastructure often cause optical sensors and LiDAR to fail, resulting in missed detections and unreliable situational awareness. Millimeter-wave (mmWave) radar, in contrast, is inherently resilient to illumination changes and particulate interference, making it a promising modality for such harsh environments.

Conventional automotive radars, however, provide only coarse angular resolution and typically lack elevation estimation, yielding sparse range–azimuth–Doppler measurements that are difficult to interpret in enclosed metallic spaces where multipath and ghost reflections are prevalent. Recent advances in *4D imaging radar* introduce elevation estimation through large virtual MIMO arrays, producing 3D point clouds enriched with Doppler and radar cross section (RCS). Although these sensors have shown promise in outdoor visibility-

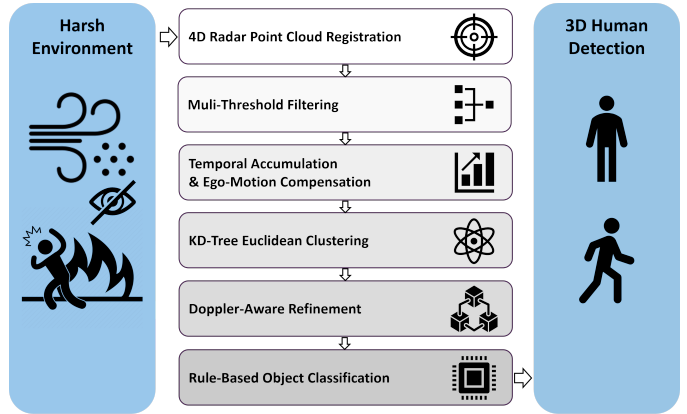


Fig. 1: Overview of the model-driven 4D radar pipeline: raw radar measurements through multi-threshold filtering, ego-motion-compensated temporal accumulation, clustering, Doppler-aware refinement, rule-based 3D classification

degraded settings, there is no established consensus on how to process their anisotropic, noise-prone point clouds in confined industrial or underground environments dominated by dust and reflective surfaces.

From this context, three specific gaps emerge:

- 1) **Sparse evaluation of 4D radar in enclosed environments with visibility degradation.** Existing studies focus primarily on outdoor automotive scenes. Radar behaviour in dust-filled, metal-walled spaces, such as industrial corridors or underground tunnels, remains largely uncharacterized.
- 2) **Limited development of radar-specific point-cloud processing pipelines.** Compared with extensive research on optical and LiDAR perception in adverse weather, far fewer works investigate radar-specific filtering, Doppler conditioning, and cluster-level reasoning tailored to 4D radar noise characteristics.
- 3) **Need for strong, interpretable model-driven baselines.** The rapid emergence of learning-based radar detectors underscores the need for lightweight, physics-motivated baselines that operate reliably in harsh enclosed environments and provide stable targets for future learning-based extensions.

To address these gaps, this paper proposes a **fully model-**

driven 4D radar perception framework for real-time human detection in industrial and underground scenarios. The system uses 4D radar as its *only perception modality*, while relying on external LiDAR–IMU odometry solely for ego-motion compensation and on LiDAR/camera data only for visualization and baseline comparison.

The main contributions of this work are:

- **A radar-only, model-driven 4D perception pipeline** tailored for enclosed dusty and metallic environments, filling a gap left by prior work focused on outdoor driving, sensor fusion, or learning-based detectors.
- **A domain-aware multi-threshold filtering module** using RCS bounds, angular constraints, and Doppler plausibility to suppress multipath and clutter common in confined spaces.
- **A lightweight two-frame temporal accumulation scheme** that uses external LiDAR–IMU odometry solely for ego-motion compensation, improving spatial consistency while keeping the system real-time and embedded-friendly.
- **A Doppler-aware clustering and deterministic 3D classifier** that infers object type, motion state, and line-of-sight movement without training.
- **Experimental validation in controlled dust and underground tunnels**, demonstrating—*in our tested scenarios*—that 4D radar maintains stable pedestrian detection where camera and LiDAR sensing are severely degraded.

II. RELATED WORK

A. Perception in Adverse Environments

Optical and LiDAR-based perception degrades sharply under adverse visibility conditions such as rain, fog, airborne dust, and low light. Numerous studies report substantial losses in detection and tracking performance even with advanced enhancement models [1], [2]. LiDAR suffers from attenuation, backscatter, and spurious returns that reduce point-cloud completeness [3]. These limitations intensify in confined or underground spaces where metallic infrastructure creates strong multipath and where maintaining situational awareness is intrinsically challenging [4]. These trends motivate sensing modalities that remain reliable when optical pathways collapse.

B. Conventional Automotive Radar

Automotive mmWave radars (76–81 GHz) provide robust range and Doppler estimates and are widely deployed for highway safety [5], [6]. However, limited antenna aperture yields coarse angular resolution and no direct elevation estimate. Standard radar outputs provide sparse range–azimuth–Doppler detections rather than full 3D structure, and their performance deteriorates in enclosed metallic environments due to multipath, ghost reflections, and anisotropic lobes [7]. These constraints limit the applicability of conventional radar to object-level perception in industrial or underground spaces.

C. 4D Imaging Radar and Existing Datasets

Recent 4D mmWave imaging radars provide elevation estimation through large virtual MIMO arrays, generating anisotropic 3D point clouds enriched with Doppler and RCS [8]. This capability has inspired several learning-based perception studies and datasets. TJ4DRadSet [9] and View-of-Delft (VoD) [10] provide radar, camera, and LiDAR data for outdoor autonomous driving, including rain and artificial fog scenarios. Other works examine radar–camera fusion or deep networks for pedestrian detection [11].

However, these datasets and methods share two key limitations. First, their adverse-weather scenes are dominated by water-based fog or smoke and occur in wide outdoor spaces. They do not capture the unique behavior of mmWave radar in confined, dust-filled, metallic environments where cavity propagation, strong multipath, and sparse returns differ fundamentally from outdoor driving settings. Second, most perception pipelines rely on learning-based models or radar–camera fusion, which require large labeled datasets and are difficult to deploy on lightweight embedded hardware.

D. Classical Geometric Pipelines

Traditional geometric pipelines rely on nearest-neighbour search, clustering, and principal-component analysis for bounding-box estimation [12]. Euclidean clustering with KD-tree acceleration is widely used for LiDAR processing [13], but such methods assume relatively dense and isotropic point clouds. In contrast, 4D radar returns are sparse and anisotropic, and their Doppler information is rarely exploited in classical frameworks.

E. Novelty and Positioning of This Work

Compared with prior research, this work differs in three fundamental ways:

- 1) **Environment:** Prior 4D radar studies focus on outdoor autonomous driving, whereas this work targets enclosed, dust-filled, metallic environments representative of industrial and underground operations.
- 2) **Modality and independence from vision:** Unlike radar–camera fusion or deep-learning detectors that require labeled datasets, our framework uses radar as the *sole perception modality*, relying only on external odometry for motion compensation.
- 3) **Model-driven, lightweight design:** Existing methods often employ heavy learning pipelines. We introduce a fully model-driven radar pipeline that integrates physically interpretable filtering, Doppler-aware clustering, and rule-based 3D classification for real-time performance on embedded hardware.

To our knowledge, this is the first work to demonstrate a fully model-driven, radar-only 4D perception framework operating in enclosed, dust- and metal-filled industrial environments, without any reliance on optical modalities or supervised learning.

III. METHODOLOGY

A. 4D Radar Platform and Multi-Sensor Setup

The 4D mmWave imaging radar used in this work is a cascaded four-chip device equipped with 12 transmit (TX) and 16 receive (RX) antennas arranged into a large virtual MIMO array capable of resolving range, azimuth, elevation, and Doppler [14]. Manufacturer specifications list azimuth and elevation resolutions on the order of 1–2° and pedestrian detection ranges of approximately 200 m; these values serve only as context, as all analysis relies on empirical measurements collected in our experiments.

Radar data are acquired using the vendor’s ROS driver, which receives UDP packets, decodes the raw range–angle–Doppler detections, converts them into Cartesian coordinates, and publishes the resulting elevation-resolved radar point cloud as `sensor_msgs/PointCloud2` at 15 Hz. Logging and timestamping are performed on an NVIDIA Jetson Orin NX edge computer. Extrinsic calibration between radar, LiDAR, and the IMU is maintained within the ROS `tf` tree (`radar→base_link→world`), ensuring consistent geometric registration across all sensors.

The radar is rigidly co-mounted with a 40-line LiDAR and an infrared (IR) camera. LiDAR provides geometric reference and supplies LiDAR–IMU odometry used exclusively for ego-motion compensation; it does not participate in perception or decision-making. The IR camera documents visibility degradation and serves only as a qualitative baseline. All perception outputs in this work are derived solely from the 4D radar point clouds.

Each radar point is represented as

$$\mathbf{p}_i = (x_i, y_i, z_i, v_i^{\text{dop}}, \text{RCS}_i, \delta_i), \quad (1)$$

where (x_i, y_i, z_i) are Cartesian coordinates, v_i^{dop} is radial Doppler velocity, RCS_i is radar cross section, and δ_i is a vendor-supplied dynamic/static flag. Indoor radar frames typically contain 3 000–6 000 points.

B. Domain-Aware Multi-Threshold Filtering

The first processing stage removes spurious radar points arising from diffuse reflections, metallic multipath, and implausible Doppler measurements. Two threshold profiles are used:

Indoor profile: strict angular and RCS limits to suppress wall- and ceiling-induced multipath in enclosed spaces (e.g., azimuth $[-5, 5]^\circ$, elevation $[-2, 8]^\circ$, RCS $[0, 45]$).

Outdoor profile: wider angular and RCS bounds to accommodate long-range reflections and broader operational coverage (e.g., azimuth $[-15, 15]^\circ$, elevation $[-6, 12]^\circ$, RCS $[-5, 55]$).

Each raw radar point \mathbf{p}_i is subjected to three filters.

a) 1) *RCS thresholding*.: Very weak diffuse returns and extremely strong multipath-induced peaks are rejected:

$$\text{RCS}_{\min} < \text{RCS}_i < \text{RCS}_{\max}. \quad (2)$$

b) 2) *Angular bound filtering*.: Azimuth θ_i and elevation ϕ_i must lie within the radar’s valid field of view:

$$\theta_i \in [\theta_{\min}, \theta_{\max}], \quad \phi_i \in [\phi_{\min}, \phi_{\max}]. \quad (3)$$

Points outside these bounds are frequently associated with ceiling/floor multipath or grazing-angle reflections.

c) 3) *Doppler plausibility filtering*.: Points with Doppler velocities inconsistent with human or machinery motion, or zero-Doppler points in locations not physically associated with static structures, are removed:

$$v_{\min} \leq v_i^{\text{dop}} \leq v_{\max}. \quad (4)$$

The resulting filtered set is

$$\begin{aligned} \mathcal{P}_{\text{filtered}} = \{ \mathbf{p}_i \in \mathcal{P}_{\text{raw}} \mid & \text{RCS}_{\min} < \text{RCS}_i < \text{RCS}_{\max}, \\ & \theta_i \in [\theta_{\min}, \theta_{\max}], \phi_i \in [\phi_{\min}, \phi_{\max}], \\ & v_i^{\text{dop}} \in [v_{\min}, v_{\max}] \}, \end{aligned} \quad (5)$$

executed in $\mathcal{O}(n)$ time per frame. This significantly reduces downstream fragmentation during clustering.

C. Temporal Accumulation with Ego-Motion Compensation

Radar point clouds are sparser than LiDAR and may contain only a few points per pedestrian in each frame. To improve spatial continuity while maintaining real-time performance, we accumulate **exactly two** consecutive frames.

Odometry is provided by FAST-LIO [15], a tightly coupled LiDAR–IMU fusion system that outputs six-degree-of-freedom poses at high frequency on a ROS `/odom` topic. These poses are used solely to (i) compensate for ego-motion when aligning radar frames and (ii) compute the platform velocity \mathbf{v}_{ego} used in Doppler correction. Radar perception itself remains radar-only.

Let \mathcal{P}_t and \mathcal{P}_{t-1} denote the filtered radar point clouds at consecutive timestamps. The transform $\mathbf{T}_{t-1}^t \in SE(3)$ maps points from the $(t-1)$ frame to the t frame. Because odometry updates run faster than radar frames, poses are time-synchronized and interpolated to radar timestamps.

The previous cloud is transformed as:

$$\mathcal{P}_{t-1}^t = \{ \mathbf{T}_{t-1}^t \mathbf{p}_i \mid \mathbf{p}_i \in \mathcal{P}_{t-1} \}, \quad (6)$$

and the accumulated cloud becomes:

$$\mathcal{P}_{\text{acc}} = \mathcal{P}_t \cup \mathcal{P}_{t-1}^t. \quad (7)$$

The two-frame window improves spatial consistency without noticeable latency and without accumulating drift. Because the radar does not strongly sense the ground, no ground-plane removal or voxel downsampling is required.

D. KD-Tree Euclidean Clustering and Doppler-Aware Filtering

Let $\mathcal{P}_{\text{acc}} = \{\mathbf{p}_i\}_{i=1}^N$. A KD-tree is constructed over the spatial coordinates (x_i, y_i, z_i) to enable neighbour queries in $\mathcal{O}(\log N)$ time.

a) *Euclidean clustering*.: Clusters $\{\mathcal{C}_1, \dots, \mathcal{C}_K\}$ are generated via radius-based connected components:

$$\|\mathbf{p}_i - \mathbf{p}_j\|_2 < d_{\text{th}} \Rightarrow \mathbf{p}_i, \mathbf{p}_j \in \mathcal{C}_k, \quad (8)$$

with overall complexity $\mathcal{O}(N \log N)$. Although originally designed for dense, isotropic LiDAR, Euclidean clustering performs reliably here because (i) strict filtering removes multipath noise, (ii) temporal accumulation increases local density, and (iii) confined indoor geometry produces compact, spatially coherent radar returns. In our experiments, we set $d_{\text{th}} = 0.6m$ (comparable to half a human torso width at typical ranges) and require at least 3 points per cluster to avoid noise.

b) *Cluster descriptors*.: For each cluster \mathcal{C}_k , we compute:

(1) Mean Doppler:

$$\bar{v}_k = \frac{1}{|\mathcal{C}_k|} \sum_{\mathbf{p}_i \in \mathcal{C}_k} v_i^{\text{dop}}. \quad (9)$$

(2) Ego-motion-compensated mean Doppler:

$$\begin{aligned} \hat{\mathbf{r}}_i &= \frac{(x_i, y_i, z_i)}{\|(x_i, y_i, z_i)\|_2}, \\ \bar{v}_k^{\text{comp}} &= \frac{1}{|\mathcal{C}_k|} \sum_{\mathbf{p}_i \in \mathcal{C}_k} \left(v_i^{\text{dop}} - \mathbf{v}_{\text{ego}} \cdot \hat{\mathbf{r}}_i \right). \end{aligned} \quad (10)$$

(3) Modal RCS:

$$\text{RCS}_{\text{mode}, k} = \text{mode}\{\text{RCS}_i : \mathbf{p}_i \in \mathcal{C}_k\}. \quad (11)$$

c) *Cluster retention*.: A cluster is retained if

$$|\bar{v}_k^{\text{comp}}| > v_{\text{min}} \quad \text{or} \quad \text{RCS}_{\text{mode}, k} \in [\text{RCS}_{\text{min}}, \text{RCS}_{\text{max}}]. \quad (12)$$

The Doppler criterion eliminates static structures, while the RCS criterion preserves both moving pedestrians and strong reflective objects.

E. Rule-Based 3D Object Classification

Each retained cluster \mathcal{C}_k^* is assigned semantic properties using three descriptors:

a) *Type inference*.: Cluster dimensions (w_k, l_k, h_k) are derived from its bounding box. Pedestrians typically exhibit widths of 0.5–1.0 m, heights below 2 m, and moderate RCS near 0; larger metallic objects exhibit both larger extents and higher RCS. Thresholds were tuned on a small validation subset and fixed for all experiments.

b) *Motion state*.: The magnitude of $|\bar{v}_k^{\text{comp}}|$ indicates whether the object is static or dynamic.

c) *Heading (line-of-sight only)*.: The sign of \bar{v}_k^{comp} indicates whether the object is approaching or receding along the radar line-of-sight. This is not a full 3D heading estimate but provides actionable situational awareness in confined environments.

The resulting classifier is deterministic, training-free, and runs in $\mathcal{O}(K)$ per frame, supporting real-time embedded deployment.

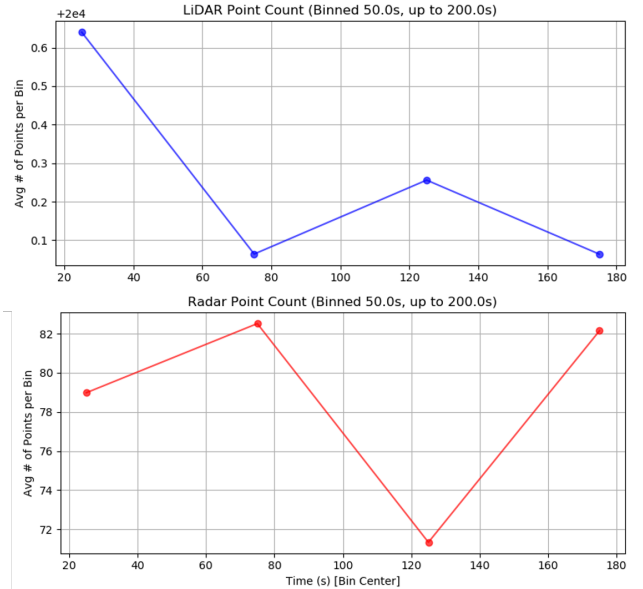


Fig. 2: Average point count per sensor under increasing dust concentration. LiDAR returns decline sharply due to attenuation and backscatter, while 4D radar maintains a nearly constant point count with only minor fluctuations, confirming robustness to particulate interference.

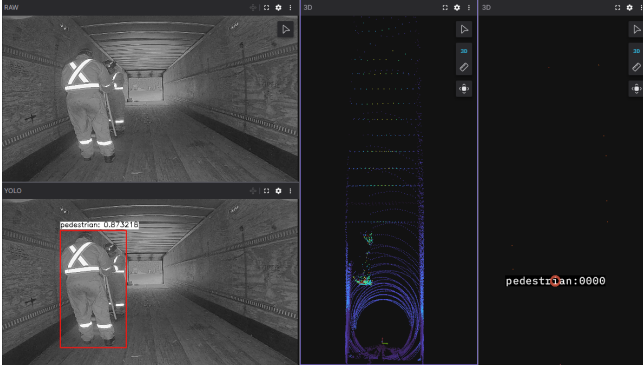
IV. EXPERIMENTS

This section evaluates the proposed model-driven 4D radar perception framework under two complementary settings: a controlled dust-filled environment enabling repeatable stress testing, and an active underground mine demonstrating real-world generalization. Evaluation focuses on (i) sensor-level robustness under degraded visibility, (ii) object-level detection stability compared with a vision-based detector, and (iii) qualitative performance in challenging industrial scenarios. These metrics provide a meaningful proof of concept without requiring dense 3D annotations, which are impractical for 4D radar due to sparse, anisotropic scattering and ambiguous spatial extents.

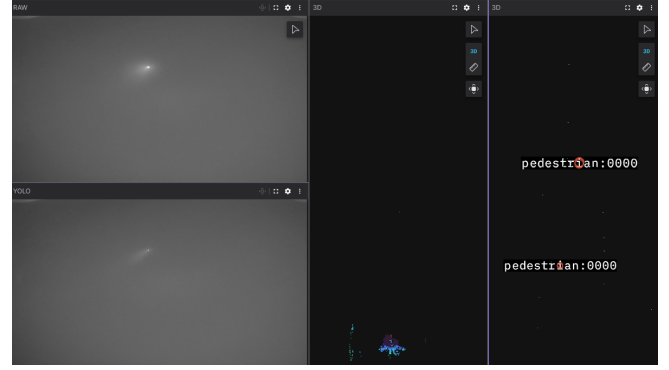
A. Controlled Dust-Filled Trailer Dataset

Experiments were conducted inside a $53' \times 10' \times 11'$ enclosed trailer configured as a controlled test chamber. Wooden walls, ceiling beams, and regularly spaced metal strips created structured but interpretable reflective surfaces while avoiding excess diffuse multipath. The corridor-like geometry emulates narrow industrial tunnels and underground passages.

A sand-based particulate mixture was dispersed to generate progressively increasing visibility degradation, from clear conditions (Dust Level 0) to heavy dust saturation. Two participants wearing high-visibility personal protective equipment moved throughout the space, producing both dynamic and near-zero-Doppler scenarios relevant for safety applications. Radar point clouds, LiDAR scans, and infrared (IR) images were synchronized using ROS, ensuring consistent timestamp alignment across modalities. No LiDAR or camera information is used for perception, classification, or decision logic.



(a) Clear environment (Dust Level 0).



(b) Highest dust concentration.

Fig. 3: Qualitative detection results under varying dust conditions. Left: Under clear conditions, IR camera, LiDAR, and radar all provide consistent structure, and both camera-based and radar-based detectors identify pedestrians. Right: At the highest dust concentration, IR and LiDAR fail completely, while the model-driven 4D radar framework continues to detect pedestrians robustly.

Figure 2 summarizes the average number of returns per sensor as dust concentration increases. LiDAR point density drops sharply due to attenuation and backscatter, whereas the 4D radar maintains nearly constant point density with only minor fluctuations. This confirms that the mmWave modality remains structurally informative even under severe particulate interference.

Annotation considerations.: The dataset does not include 3D bounding-box annotations. Radar measurements exhibit sparse, anisotropic point distributions dominated by specular and multipath reflections, preventing reliable spatial annotation. Constructing a large fully annotated 4D radar dataset would require specialized tools and substantial labor, which is outside the scope of this work. Instead, evaluation emphasizes objective, interpretable metrics: sensor-level robustness, high-level detection stability, and deployability on embedded hardware.

B. Model-Driven Radar vs. Camera-Based Detection

We compare the proposed radar-only classifier against a YOLOv8 camera-based detector [16] pretrained on the Construction Site Safety dataset [17]. Both methods process synchronized ROS data streams and attempt to detect pedestrians as dust levels increase.

Figure 4 shows the number of pedestrians detected over time. In clear conditions, both detectors operate reliably. As dust concentration rises, IR imagery becomes heavily obscured and YOLOv8 fails abruptly. In contrast, the radar-based classifier remains stable across all dust levels due to its reliance on mmWave reflections.

Quantitative comparison.: To complement the qualitative observations, we performed a lightweight but objective statistical analysis using a short segment of synchronized radar and camera data in which two pedestrians were continuously present across all 160 frames. The evaluation is conducted using *count-based metrics* that require no spatial labels due to the lack of annotations: (i) frame-wise recall, indicating whether at least one pedestrian was detected in a given frame; (ii) person-count recall, comparing the number of detected

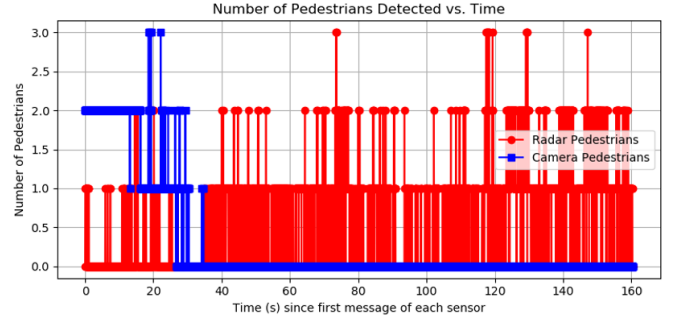


Fig. 4: Pedestrian detections over time from the model-driven radar classifier (red) and a YOLOv8 camera detector (blue). As dust levels increase, camera-based detection collapses, whereas radar detection remains stable.

TABLE I: Quantitative pedestrian-detection results in a two-person sequence (160 frames)

Metric	Radar (Ours)	YOLOv8 (Camera)
Frame-wise recall	150/160 (94%)	27/160 (17%)
Person-count recall	270/320 (84%)	40/320 (12.5%)
False-alarm rate	~5% of frames	~3% of frames

individuals against the known two-person ground truth; and (iii) false-alarm rate, measuring frames in which the detector overestimates the number of pedestrians. These metrics directly capture temporal stability and robustness under dust without relying on annotation-heavy pipelines.

These results show a clear performance gap: while the camera-based detector fails in most frames due to dust-induced visibility loss, the radar-based pipeline retains high recall and only minor count overestimation caused by cluster fragmentation. The qualitative sequences in Figs. 3a–3b reinforce this behavior: under severe dust saturation, both the IR camera and LiDAR become unusable, yet the 4D radar point cloud remains sufficiently structured for consistent and reliable pedestrian detection.

C. Underground Mining Scenario

To evaluate generalization beyond controlled environments, the same framework was deployed in an active underground

mining tunnel:

Scenario overview.: Figure 5 shows a representative frame from the underground deployment. A miner is present at approximately 60 m distance, which makes the human signature appear small in both the IR camera view and the radar visualization. Airborne dust, irregular tunnel surfaces, and severe headlamp glare substantially degrade image contrast, causing no detections from YOLO. Despite the reduced visibility and long range, the model-driven 4D radar framework consistently identifies the pedestrian by leveraging Doppler- and RCS-aware clustering, demonstrating robustness where camera-based perception collapses.



Fig. 5: Underground mining evaluation. Camera-based detection fails due to dust and headlamp glare, whereas the model-driven radar framework maintains reliable pedestrian detection.

Despite these conditions, the radar framework maintains stable detection across frames. Doppler- and RCS-aware clustering isolates the pedestrian from background multipath, demonstrating robustness in visibility-degraded, high-reflectivity environments.

V. CONCLUSION

This paper presented a fully model-driven 4D radar perception framework for robust human detection in harsh industrial and underground environments where cameras and LiDAR often fail due to airborne particulates, low visibility, and confined geometry. The proposed pipeline operates exclusively on 4D mmWave radar point clouds and combines domain-aware multi-threshold filtering, two-frame ego-motion-compensated accumulation, Doppler-aware clustering, and a lightweight rule-based classifier. The system is designed for real-time execution on embedded platforms and requires no supervised training.

Experiments in a controlled dust-filled trailer and a real underground mining tunnel demonstrated that the 4D radar maintains a stable structure and reliable pedestrian detection under severe visibility degradation, in conditions where both vision-based YOLO detection and LiDAR returns deteriorate. These results validate the suitability of elevation-resolved radar for pervasive safety monitoring and human detection in environments dominated by dust, clutter, and irregular reflectivity.

Overall, this work establishes a clear, interpretable, and deployable baseline for radar-only perception in adverse environments, and serves as a foundation for future 4D radar research in safety-critical industrial applications.

ACKNOWLEDGEMENT

The authors of this paper would like to acknowledge the support of Rogers, LoopX, Purolator, Cloudbhawk, NSERC, MITACS, and WATCAR.

REFERENCES

- [1] Y. Qiu, Y. Lu, Y. Wang, and C. Yang, “Visual perception challenges in adverse weather for autonomous vehicles: A review of rain and fog impacts,” in *2024 IEEE 7th Information Technology, Networking, Electronic and Automation Control Conference (ITNEC)*, vol. 7, 2024, pp. 1342–1348.
- [2] Z. Chen, Z. Zhang, Q. Su, K. Yang, Y. Wu, L. He, and X. Tang, “Object detection for autonomous vehicles under adverse weather conditions,” *Expert Systems with Applications*, vol. 296, p. 128994, 2026. [Online]. Available: <https://www.sciencedirect.com/science/article/pii/S0957417425026119>
- [3] M. Dreissig, D. Scheuble, F. Piewak, and J. Boedecker, “Survey on lidar perception in adverse weather conditions,” 2023.
- [4] X. Wang, L. Shen, and S. Shi, “Evaluation of underground space perception: A user-perspective investigation,” *Tunnelling and Underground Space Technology*, vol. 131, p. 104822, 2023. [Online]. Available: <https://www.sciencedirect.com/science/article/pii/S088677982200462X>
- [5] B. van Berlo, A. Elkelany, T. Ozcelebi, and N. Meratnia, “Millimeter wave sensing: A review of application pipelines and building blocks,” *IEEE Sensors Journal*, vol. 21, no. 9, pp. 10 332–10 368, 2021.
- [6] S. M. Patole, M. Torlak, D. Wang, and M. Ali, “Automotive radars: A review of signal processing techniques,” *IEEE Signal Processing Magazine*, vol. 34, no. 2, pp. 22–35, 2017.
- [7] I. Bilik, “Comparative analysis of radar and lidar technologies for automotive applications,” *IEEE Intelligent Transportation Systems Magazine*, vol. 15, no. 1, pp. 244–269, 2023.
- [8] Z. Han, J. Wang, Z. Xu, S. Yang, L. He, S. Xu, J. Wang, and K. Li, “4d millimeter-wave radar in autonomous driving: A survey,” 2023.
- [9] L. Zheng, Z. Ma, X. Zhu, B. Tan, S. Li, K. Long, W. Sun, S. Chen, L. Zhang, M. Wan, L. Huang, and J. Bai, “Tj4dradset: A 4d radar dataset for autonomous driving,” in *2022 IEEE 25th International Conference on Intelligent Transportation Systems (ITSC)*, 2022, pp. 493–498.
- [10] A. Palfy, E. Pool, S. Baratam, J. F. P. Kooij, and D. M. Gavrila, “Multi-class road user detection with 3+1d radar in the view-of-delft dataset,” *IEEE Robotics and Automation Letters*, vol. 7, no. 2, pp. 4961–4968, 2022.
- [11] M. Skog, O. Kotlyar, V. Kubelka, and M. Magnusson, “Human detection from 4d radar data in low-visibility field conditions,” 2024. [Online]. Available: <https://arxiv.org/abs/2404.05307>
- [12] S. Kato, S. Tokunaga, Y. Maruyama, S. Maeda, M. Hirabayashi, Y. Kitayukawa, A. Monrroy, T. Ando, Y. Fujii, and T. Azumi, “Autoware on board: Enabling autonomous vehicles with embedded systems,” in *2018 ACM/IEEE 9th International Conference on Cyber-Physical Systems (ICCP)*, 2018, pp. 287–296.
- [13] Y. Miao, S. Li, L. Wang, H. Li, R. Qiu, and M. Zhang, “A single plant segmentation method of maize point cloud based on euclidean clustering and k-means clustering,” *Computers and Electronics in Agriculture*, vol. 210, p. 107951, 2023. [Online]. Available: <https://www.sciencedirect.com/science/article/pii/S0168169923003393>
- [14] A. Radar, “Altos radar product page,” <https://www.altosradar.com/product>, 2023, accessed: 2024-09-09.
- [15] W. Xu, Y. Cai, D. He, J. Lin, and F. Zhang, “Fast-lio2: Fast direct lidar-inertial odometry,” 2021.
- [16] G. Jocher, J. Qiu, and A. Chaurasia, “Ultralytics YOLO,” Jan. 2023. [Online]. Available: <https://github.com/ultralytics/ultralytics>
- [17] R. U. Projects, “Construction site safety dataset,” <https://universe.roboflow.com/roboflow-universe-projects/construction-site-safety>, aug 2024, visited on 2025-01-17. [Online]. Available: <https://universe.roboflow.com/roboflow-universe-projects/construction-site-safety>